

EXTREMUM SEEKING CONTROL FOR THE OPTIMIZATION OF HEAVY ION BEAM TRANSPORTATION

H. Fujii^{1†}, A. Scheinker², A. Uchiyama¹, S.J. Gessner³, O. Kamigaito¹
and N. Fukunishi¹

¹ Nishina Center, RIKEN, Wako, Saitama, Japan

² Los Alamos National Laboratory, Los Alamos, NM, USA

³ SLAC National Accelerator Laboratory, Menlo Park, CA, USA

Abstract

Riken Nishina Center (RNC) is currently working on automated tuning and diagnostics algorithms to enable efficient and optimal operation of its heavy ion beam accelerator complex. We applied the recently developed dither-based Extremum Seeking Control (ESC) scheme to a part of the heavy ion beam transport system to adjust beam optics. This paper briefly explains the ESC algorithm whose input states are bounded within a safe operation condition, and the results of the beam optics tuning by applying ESC algorithm to noise-corrupted observables. The robustness of ESC under noisy environment and potential applications for higher current operation while suppressing the unknown and time-varying nonlinear effects at RNC accelerator complex are also discussed.

INTRODUCTION

Established optimal tuning of a multi-stage particle accelerator complex such as Radioactive Isotope Beam Factory (RIBF) at RIKEN requires years of experience because of tight precision requirements in the face of numerous uncertainties and deviations from the original designs which include misalignments, subtle differences in material properties, and the unexpected nonlinear effects on beam dynamics. Moreover, even once the entire complex is optimized for a certain machine state, the thermal effect and subtle instabilities of ion sources affect the beam distribution. In the tuning of the RIBF accelerator complex, these effects are compensated by careful manual tuning. Although beam optics in RIBF is relatively simple, it is often difficult to handle many tuning parameters when the ion source state changes slightly. Therefore, there is a demand for “smart knobs” to achieve certain beam properties based on multiple measurement data.

Recent data-driven techniques and machine learning (ML) methods have enabled us to handle such high-dimensional systems efficiently by solving a minimization problem. The gaussian process optimizer (GP) is an instance-based learning method. It has been applied to maximize the X-ray laser pulse energy [1]. An extension of GP by constructing the kernel from the physical model’s basis-functions has also been applied to minimize the emittance in SPEAR storage ring [2]. The neural-network (NN) based surrogate models have been applied to virtually diagnose

the beam properties, and to achieve the desired beam profile based on the model [3, 4]. However supervised ML methods search broad parameter spaces and might result in damage to accelerators when unsafe tuning parameters are adopted during optimization. Especially for future application at RIBF facility, beam tuning from low intensity to its maximum intensity requires careful attention because a full power beam can easily damage the accelerator component within one second and therefore must be robust to time-varying system. Also, such ML methods require time-consuming retraining steps once the machine state shifts. In such a scenario, an adaptive controller which continuously optimizes the machine state without a drastic change in response to the noisy measurements is preferable.

Among such data-driven methods, we adopted a perturbation based extremum seeking control (ESC) algorithm [5, 6] as a first and easy-to-implement approach. The ESC minimizes a user-defined objective function of an unknown system with dithered input signals towards optimal control directions. The ESC algorithm has been applied to optimize various accelerator components with uncertainties, such as RF control [7], maximization of the X-ray FEL pulse energy [8], and simultaneously minimizing emittance growth and alignment error at AWAKE [9]. Work has begun on combining ESC with ML to automatically adjust the longitudinal phase space of beams [10]. In this report, we applied ESC for a part of the beam transport system of the AVF cyclotron of RIBF to achieve a controlled beam intensity and profile upon the target used in the RI production experiments by controlling beam spills on the baffle slits just before the RI production target. We observed the continuous decline in the adopted objective functions even under external disturbances. A problem particular to multi-objective function minimization during the experiment is explained and a solution candidate to overcome the problem is demonstrated with a simulation similar to the experiment.

EXTREMUM SEEKING CONTROL ALGORITHM

The referred ESC algorithm [7–9] is designed to minimize (or maximize) a user-defined cost function $C(\mathbf{p}, t) \in \mathbb{R}$, whose dependency to the system is unknown, but changes its value according to the change in n -parameters. $\mathbf{p} = (p_1, \dots, p_n)$, where p_i can be any of the accelerator input such as RF voltages and magnetic fields at each time t .

† hiroki.fujii@riken.jp

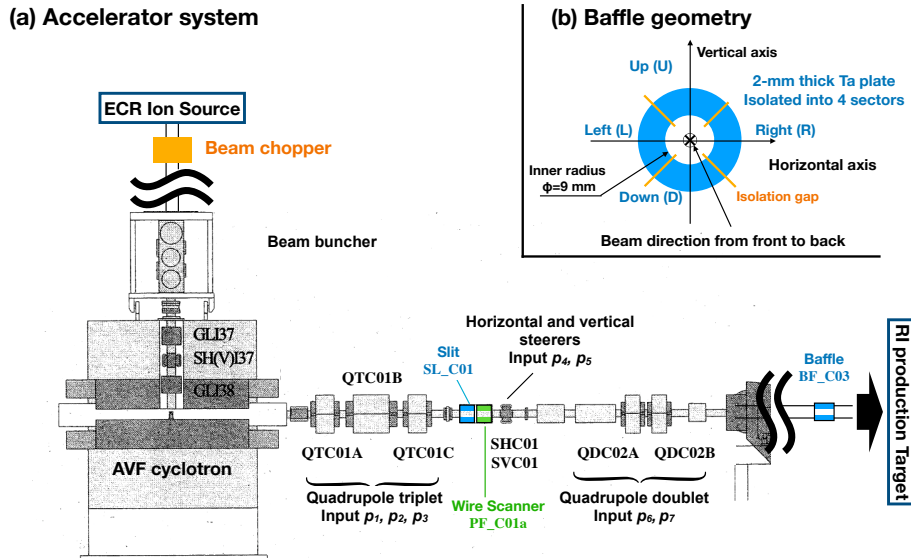


Figure 1: (a) The AVF cyclotron system where the ESC algorithm is applied. Input parameters are summarized in Table 1. (b) The geometry of the baffle (beam loss monitor) composed of 4 conductive fun-shaped tantalum plates.

The algorithm adjusts input parameters according to the dynamics

$$\frac{dp_i}{dt} = \sqrt{\alpha_i \omega_i} \cos[\omega_i t + k \hat{C}(\mathbf{p}, t)], \quad (1)$$

based on noise-corrupted measurement of the cost function $\hat{C}(\mathbf{p}, t) = C(\mathbf{p}, t) + v(t)$ where $v(t)$ is a time-varying machine noise. The dither frequencies ω_i should be differently chosen for each parameter such that one signal is orthogonal to each other in Hilbert Space in the form of the inner product $L^2[0, t]: \lim_{\omega_1, \omega_2 \rightarrow \infty} \int_0^t \cos(\omega_1 \tau) \cos(\omega_2 \tau) d\tau = 0$ ($\omega_1 \neq \omega_2$). The resulting average dynamics of Eq. (1) is

$$\frac{dp_i}{dt} = -\frac{k\alpha_i}{2} \frac{\partial C(\mathbf{p}, t)}{\partial p_i}, \quad (2)$$

resulting in minimization of the unknown cost function $C(\mathbf{p}, t)$ with respect to p_i . Later on, we denote noise

Table 1: Cosine Similarities between the Digital Input and Analog Readout Currents of the Power Supplies

Index i	Magnet name	Function	Similarity sim_i (Eq. (4))
1	QTC01A		0.16
2	QTC01B	QT cell	0.57
3	QTC01C		0.86
4	SHC01	Horizontal deflection	0.91
5	SVC01	Vertical deflection	0.76
6	QDC02A		0.59
7	QDC02B	QD cell	0.88

corrupted measurement $\hat{C}(\mathbf{p}, t)$ as $C(\mathbf{p}, t)$ for simplicity. This algorithm limits its parameter update rate to $\left| \frac{dp_i}{dt} \right| = \left| \sqrt{\alpha_i \omega_i} \cos[\omega_i t + kC(\mathbf{p}, t)] \right| \leq \sqrt{\alpha_i \omega_i}$, which is advantageous for safely optimizing the input parameters even for the noise corrupted cost function whose gradient is unknown. More detailed views of this algorithm including stability proofs and connection to the quadratic controller can be found in Ref. [6].

APPLICATION OF ESC TO THE AVF SYSTEM AT RNC

System statement and tuning objective

We applied ESC algorithm to a part of the beam transport line used for the RI production experiments. Figure 1a illustrates the system where we tested the ESC algorithm in our facility. The AVF cyclotron [11] at the left-hand side of the Fig. 1a accelerates the deuteron beams produced by ECR Ion source up to 12 MeV/u, for instance, to irradiate ^{70}ZnO target to produce ^{67}Cu radioactive isotope. The beam property at the RI production target is tuned by 7 input parameters for a controlling quadrupole triplet, horizontal and vertical steerers, and a subsequent quadrupole doublet as summarized in Table 1. The beam intensity in the RI production process should be high enough to increase the production rate while keeping the beam spot not too small in order to prevent the target from melting. However, the detector components such as baffles and wire scanners can be damaged easily by the maximum beam current available. Therefore, we first adjust beam optics to have a large enough radius confirmed by the controlled beam losses at each baffle plates (baffle currents) for a beam with its intensity attenuated by using a beam chopper, and then gradually increase the beam intensity up to its maximum value while keeping the baffle currents at each side (Fig. 1b).

This procedure has been done empirically by operators while gradually increasing beam intensity by changing the duty factor of a beam chopper installed just downstream of the ion source. Our goal here is to automate this process with the ESC algorithm and confirm the robustness against disturbances including beam intensification and manual operation for other components.

Cost function design for the ESC algorithm

In the problem stated above, we designed the evaluation function as to minimize the beam loss on the slit (SL_C01) as a safe operation condition, and also to control the beam loss signals on 4 baffles to a targeted value b ($=100$ nA in the subsequent experiment) simultaneously. As a safety objective function of the current signal on each side of the slit installed along the trajectory, we adopted the rectified linear unit (ReLU): $S_j(J_j) = \max\left(0, \frac{J_j - \mu}{\xi_s}\right)$, where subscripts $j \in \{R, L, U, D\}$ describes the direction (Right, Left, Up, Down), $J_{R,L,U,D}$ is the current on slits at each direction, ξ_s is the normalization factor, and μ is a dead-band current such that subtle noise in slit current doesn't significantly affect the overall cost function. Similarly, the baffle objective function was chosen to be the following absolute linear function:

$B_j(I_j) = \left| \frac{I_j - b}{\xi_B} \right|$, where $j \in \{R, L, U, D\}$, where I_j is the baffle current measured by each fun-shaped tantalum plate, b is the target current, and ξ_B is the normalization factor. Though this is a discontinuous objective function,

continuous objective function around the setpoint, such as Huber loss function [12], is preferred in future experiments.

The overall cost function $kC(\mathbf{p}, t) \in \mathbb{R}$ of this particular setup is a weighted sum of $S(J)$ and $B(I)$ such that

$$kC(\mathbf{p}, t) = \sum_{j=R,L,U,D} S_j(J_j(\mathbf{p}, t)) + w_j B_j(I_j(\mathbf{p}, t)) \quad (3)$$

where we introduced hyper parameters w_j to obtain better convergence for the present multi-objective function optimization, which will be discussed later in this paper. Throughout the experiment, w_j was chosen to be 1, and the objective function for slit $S_j(J_j(\mathbf{p}, t))$ were kept close to 0, and thus can be ignored throughout the following discussion.

Hyperparameter tuning and hardware issues during the experiment

In the numerical implementation below, dither frequencies ω_i ($i = 1, 2, \dots, n$) of Eq. (1) were fixed to be evenly spanned values within a set $[1, 1.75]$ such that $\Delta\omega = \omega_i - \omega_{i-1} = 0.75/(n-1)$, and parameters are updated according to Eq. (1) at every discrete time step $T = 2\pi/(10 \max \omega_i)$. The initial oscillation amplitudes $\sqrt{\alpha_i \omega_i}$ of each dithered input signal p_i is determined empirically by observing if a detectable dither on baffles can be observed and defined to update the parameters between the lower and upper bounds for the machine protection. The oscillation amplitude is designed to decay by a factor of $\gamma = 0.999$ every discrete time step T so that the input dither amplitudes gradually diminish. Each step took typically 2 seconds in this experiment.

We run this algorithm on a python script and interfaced the controller value and readout value via EPICS' IOCs. One problem we encountered here is that some old controllers used for magnet power supplies sometimes fail its communication with the EPICS' IOC, which is illustrated in Fig. 2, where the analog readouts converted by ADCs (p_{ADC}) do not follow sinusoidal digital-input values (p_{DAC}) faithfully. The cosine similarity index between the analog readout and the digital input is defined as

$$sim_i(\mathbf{p}_{ADC_i}, \mathbf{p}_{DAC_i}) = \frac{\mathbf{p}_{ADC_i} \cdot \mathbf{p}_{DAC_i}}{\|\mathbf{p}_{ADC_i}\| \|\mathbf{p}_{DAC_i}\|} \quad (4)$$

where we defined the time-series measurements of the i -th component of the analog readout current as $\mathbf{p}_{ADC_i} = [p_{ADC_i}(T), p_{ADC_i}(2T), \dots, p_{ADC_i}(MT)] \in \mathbb{R}^M$ and the digitally applied input current as $\mathbf{p}_{DAC_i} = [p_{DAC_i}(T), p_{DAC_i}(2T), \dots, p_{DAC_i}(MT)] \in \mathbb{R}^M$ for the discrete time steps of the ES algorithm $t = mT$ ($m = 1, 2, \dots, M$). For the ideal performance, the cosine similarity index should correspond to one for all the input parameters. The indices $sim_i(\mathbf{p}_{ADC_i}, \mathbf{p}_{DAC_i})$ for the particular case in

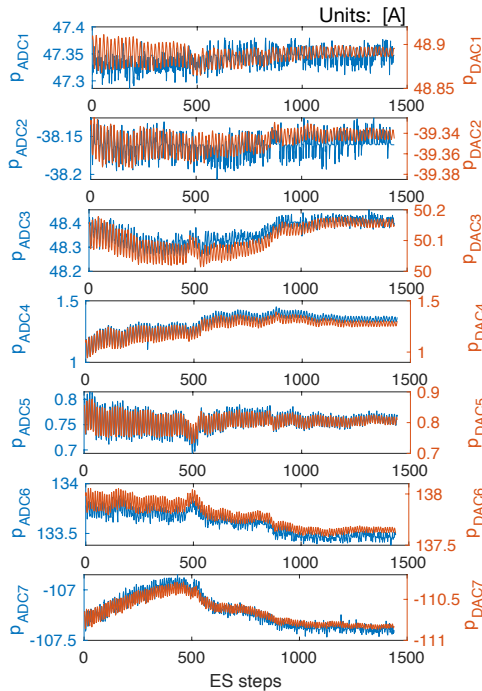


Figure 2: Comparison between the digital input and analog readout signal from the power supply controllers of all the inputs p_i ($i = 1, 2, \dots, 7$) in Table 1. The similarities of these signals are characterized by Eq. (3).

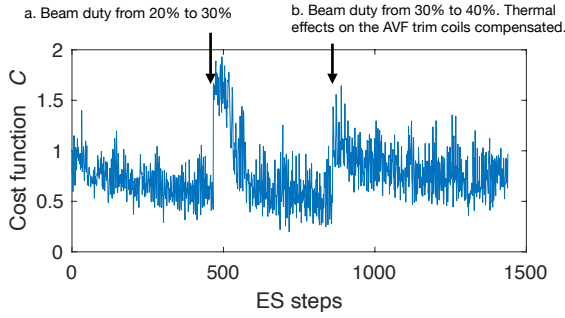


Figure 3: The overall cost function defined by Eq. (3) as a result of the input parameters in Fig. 2.

Fig. 2 are summarized in Table 1. The results of the calculation in Table 1 indicate that the error rates in the communication of some components (especially p_1) were not suffice enough for a trustful operation of the ESC algorithm while other indices are at least $sim_i > 0.5$ or larger. In the tuning process of the oscillation amplitude $\sqrt{\alpha_i \omega_i}$, we were aware of the erroneous behavior of the first component p_1 and thus decreased its oscillation amplitude low enough to make it less sensitive on overall evaluation function. This hardware issue should be investigated before applying ESC in the future applications both by replacing old components and by detecting the faulty operations.

Detailed view of the multi-objective evaluation function

One of the experimental results for the overall cost function $C(\mathbf{I}(\mathbf{p}, t), \mathbf{J}(\mathbf{p}, t))$ (Eq. (3)) with the input parameters in Fig. 2 is shown in Fig. 3. The overall cost function is decreasing continuously by adjusting the beam optics. The sudden increases at around 450 steps (labeled as (a)) and 850 steps (labeled as (b)) are because of the increment of the beam intensity by changing the duty factor of the beam chopper from 20% to 30% and from 30% to 40%, respectively. The manual tuning of main coils of AVF cyclotron magnet is also appropriately performed to compensate for the thermal drift during the test of the algorithm.

Although the overall cost function continuously decreasing throughout the experiment, each baffle current, especially the left one, is not simultaneously controlled to the setpoint $b = 100$ [nA] when $w_j = 1$ because of the too small fluctuation in its baffle current as shown in Fig. 4, where the variation of I_L is much smaller than other 3 components while 400 steps within the ESC loop. One possible reason of this small I_L fluctuation in the baffle current is because of the skewed beam profile as shown in Fig. 5, which is a result of the large energy spread of the beam extracted from the AVF cyclotron. The observed large right-and-left asymmetry of the beam profile causes different number of tail particles detected by the baffles when magnets work as to deflect the beam horizontally. This fact motivates to introduce an adaptive update scheme of the weight w_j in Eq. (3).

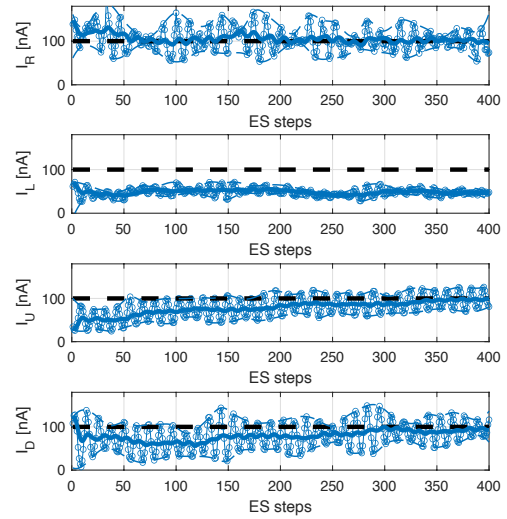


Figure 4: The measured beam losses on the baffle $I_{R,L,U,D}$ are described by circles associated with thin solid lines. Black dashed lines are setpoint currents. Two thin blue dashed lines below and above the measurements are drawn to guide your eyes for envelopes of the measurements. Thick blue lines in the middle are 20-steps averaged current signals.

IN-SITU ADAPTIVE WEIGHTING FOR THE MULTI-OBJECTIVE FUNCTION OPTIMIZATION

One way to adaptively weight objective functions B_j , depending on their sensitivity to the overall cost function, is to update the weights w_j based on a set of past fluctuation history of objective functions $B_j(I_j)$. Let $\mathbf{B}_j(I_j) \in \mathbb{R}^N$ a past $N (> 2\pi/\omega_j)$ steps of time-series measurement data of objective function, and $\bar{\mathbf{B}}_j(I_j) \in \mathbb{R}^N$ a simple moving average of $\mathbf{B}_j(I_j)$. Then, the magnitude of dithers can be characterized by subtracting the simple moving average from the original objective function, and taking the variance of it: $\sigma_{B_j}^2 = V(\mathbf{B}_j(I_j) - \bar{\mathbf{B}}_j(I_j))$, where $V(\mathbf{x})$ is the variance of \mathbf{x} . Since the ESC algorithm is empirically stable when the variance of phase kC is about 0.5^2 , we may update the weighting factor $\mathbf{w} = \{w_j | j = R, L, U, D\}$ every N samples according to $\widehat{w}_j^2 = 0.5^2 / \sigma_{B_j}^2$. Then, the updated vector $\widehat{\mathbf{w}} = \{\widehat{w}_j | j = R, L, U, D\}$ was rescaled to $\mathbf{w}_{new} = \eta \widehat{\mathbf{w}}$ by a scalar $\eta (\leq 1.5)$ so that the L^1 norm satisfies the condition $\|\mathbf{w}_{new}\|_1 \leq 1.5 \|\widehat{\mathbf{w}}\|_1$ for regulating the abrupt change after each update. Here, factor 1.5 is also empirically chosen by simulations, but the asymptotic stability may better be discussed based on the magnitude of noise. To investigate effectiveness of this scheme, we pre-configured a numerical simulation using similar geometry as in the experiment, and by initializing a skewed-gaussian profile in the transverse direction with 10,000 macroparticles. In Fig. 6a, the result of macroparticles observed at

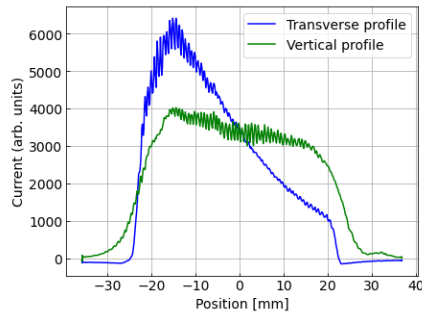


Figure 5: Typical beam profile measured by the wire scanner PF_C01 in Fig. 1.

each baffle without the adaptive weighting scheme is shown, where baffle B_U and B_D has higher sensitivities than B_R and B_L . In Fig. 6b, the adaptive weighting with $N = 200$ data is introduced for the same configuration in Fig. 6a, and we observed that all baffle currents are controlled to around a setpoint within much earlier steps. In the simulation, we also introduced an amplification of $\sqrt{\alpha_i \omega_i}$ by a factor $1/\gamma^{2N}$ when the overall cost function increases every N steps to keep the decaying dither signal on the cost function above the magnitude of noise throughout the simulation, and confirmed stable control of baffle currents for at least 10 thousand steps. These features will be tested in future experiments.

SUMMARY

In this paper, we summarized the application of ESC algorithm to a part of RNC accelerator complex whose model is unknown. The ESC algorithm led the machine state toward minimizing the given noisy evaluation function even under the external tuning applied during its operation and despite the faulty behavior of some controller components. In-situ adaptive weighting scheme of multi-objective cost function was developed and tested numerically for the faster convergence for less sensitive objects in the multiple-objective case.

ACKNOWLEDGEMENTS

The authors are grateful to the SHI Accelerator Service Ltd., especially to Ryo Koyama and Makoto Nishimura, for help with operation experiences and archiving data. We would also like to thank to Prof. Masaki Yamakita, whose comments and suggestions throughout the course of our study were of immeasurable value.

REFERENCES

- [1] J. Duris *et al.*, “Bayesian Optimization of a Free-Electron Laser,” *Phys. Rev. Lett.*, vol. 124, no. 12, p. 124801, Mar. 2020.
- [2] A. Hanuka *et al.*, “Physics model-informed Gaussian process for online optimization of particle accelerators,” *Phys. Rev. Accel. Beams*, vol. 24, no. 7, p. 072802, Jul. 2021.

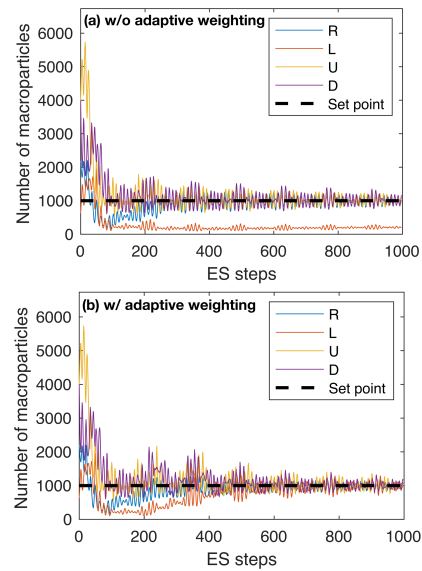


Figure 6: Numerical simulation for the similar setup in (above) without and (below) with the adaptive weighting scheme based on the past $N = 200$ measurement data.

- [3] A. Edelen, N. Neveu, M. Frey, Y. Huber, C. Mayes, and A. Adelman, “Machine learning for orders of magnitude speedup in multiobjective optimization of particle accelerator systems,” *Phys. Rev. Accel. Beams*, vol. 23, 2020.
- [4] C. Emma, A. Edelen, M. J. Hogan, B. O’Shea, G. White, and V. Yakimenko, “Machine learning-based longitudinal phase space prediction of particle accelerators,” *Phys. Rev. Accel. Beams*, vol. 21, no. 11, p. 112802, Nov. 2018.
- [5] A. Scheinker and D. Scheinker, “Bounded extremum seeking with discontinuous dithers,” *Automatica*, vol. 69, pp. 250–257, Jul. 2016.
- [6] A. Scheinker and D. Scheinker, “Extremum seeking for optimal control problems with unknown time-varying systems and unknown objective functions,” *Int. J. Adapt. Control Signal Process.*, vol. 35, no. 7, pp. 1143–1161, Jul. 2021.
- [7] A. Scheinker, “Application of Extremum Seeking for Time-Varying Systems to Resonance Control of RF Cavities,” *IEEE Trans. Control Syst. Technol.*, 2017.
- [8] A. Scheinker *et al.*, “Model-independent tuning for maximizing free electron laser pulse energy,” *Phys. Rev. Accel. Beams*, vol. 22, no. 8, p. 082802, Aug. 2019.
- [9] A. Scheinker *et al.*, “Online multi-objective particle accelerator optimization of the AWAKE electron beam line for simultaneous emittance and orbit control,” *AIP Adv.*, vol. 10, no. 5, p. 055320, May 2020.
- [10] A. Scheinker, A. Edelen, D. Bohler, C. Emma, and A. Lutman, “Demonstration of Model-Independent Control of the Longitudinal Phase Space of Electron Beams in the Linac-Coherent Light Source with Femtosecond Resolution,” *Phys. Rev. Lett.*, vol. 121, no. 4, p. 044801, Jul. 2018.
- [11] K. Suda *et al.*, “Status Report of the Operation of the RIKEN AVF Cyclotron,” *HIAT2015 Proceedings*, Yokohama, Japan, 2016.
- [12] P. J. Huber, “Robust Estimation of a Location Parameter,” *Ann. Math. Stat.*, vol. 35, no. 1, pp. 73–101, Mar. 1964.